Lab on a Chip

PAPER

View Article Online
View Journal

Cite this: DOI: 10.1039/c5lc00731c

Paper diagnostic device for quantitative electrochemical detection of ricin at picomolar levels†

Josephine C. Cunningham,[a] Karen Scida,[a] Molly R. Kogan,[a] Bo Wang,[b] Andrew D. Ellington[b] and Richard M. Crooks*[a]

Received 25th June 2015,
Accepted 20th July 2015

DOI: 10.1039/c5lc00731c

www.rsc.org/loc

We report a paper-based assay platform for detection of ricin *a* chain. The paper platform is assembled by simple origami paper folding. The sensor is based on quantitative, electrochemical detection of silver nanoparticle labels linked to a magnetic microbead support *via* a ricin immunosandwich. Importantly, ricin was detected at concentrations as low as 34 pM. Additionally, the assay is robust, even in the presence of 100-fold excess hoax materials. Finally, the device is easily remediated after use by incineration. The cost of the device, not including reagents, is just $0.30. The total assay time, including formation of the immunosandwich, is 9.5 min.

Introduction

Point-of-need analytical devices are important for quickly detecting chemical and biological weapons. Here we report a low-cost, appropriately sensitive three-dimensional (3D) paper diagnostic device for quantitative detection of the biological threat agent ricin. The sensor is based on a paper fluidic platform that incorporates a high-affinity antibody sandwich assay with electrochemically-amplified detection. Because the primary source of amplification is oxidation of silver nanoparticles (AgNPs), no enzymes are required. This results in a more robust and faster assay than is normally possible using enzymatic amplification, but the sensor described here still yields picomolar detection limits.

The detection of biological warfare agents is typically carried out in a laboratory setting using mass spectrometry or automated polymerase chain reaction (PCR) instrumentation.[1] However, impressive advances have been made for rapid detection (within 30 min) of biological warfare agents using handheld readers. For example, QTL Biosystems developed an instrument for ricin detection that was based on fluorescence quenching.[2,3] Other commercial point-of-need detection strategies for ricin incorporate colorimetry,[4] electrochemiluminescence,[5,6] and fluorescence.[7]

3D paper fluidic devices were first reported by Whitesides and colleagues[8] and hold great potential as point-of-need platforms. Since 3D paper analytical devices (PADs) were first reported, they have evolved into quite sophisticated detection platforms while maintaining their simplicity and low cost. The most common detection methods used for 3D PADs are colorimetry, flow-time measurement, and electrochemistry. Colorimetry dominates the PAD field and has been used to detect small molecules,[9–11] viruses,[12] metals,[13,14] bacteria,[15] and proteins[9,16,17] in urine,[17] natural waters,[14] and serum.[11] Detection limits are typically in the low micromolar range.[10,14–16] The Phillips group used flow time for quantitative detection of enzymes[18] and molecules[18,19] by implementing analyte-specific hydrophobic to hydrophilic fluidic switches.[19] For active enzymes, detection limits in the femtomolar range have been demonstrated.[18]

Electrochemical detection in 3D PADs can be particularly advantageous because of its simplicity, low power requirements, low limits of detection, and ease of quantitation.[20] Electrochemical detection has been demonstrated for an impressive list of analytes, including: ions,[21,22] proteins,[23,24] metals,[13,25] molecules,[25–28] biomarkers,[29,30] gases,[31] and DNA[32,33] down to low picomolar levels.[33] Generally buffer has been used as the sample medium, but in some cases detection was carried out in serum[29] or natural waters.[28]

Metal nanoparticles have been used as labels for immunoassays for some years. The detection methods they enable include plasmonics,[34,35] colorimetry,[36] and electrochemistry.[37,38]

[a] *Department of Chemistry, The University of Texas at Austin, 105 E. 24th St., Stop A5300, Austin, TX, 78712 USA. E-mail: crooks@cm.utexas.edu; Tel: 512 475 8674*

[b] *Department of Microbiology, The University of Texas at Austin, 2500 Speedway, MBB 3.424, Austin, TX, 78712 USA*

† Electronic supplementary information (ESI) available: A description of the conventional electrochemical cell; the *o*Slip fabrication procedure; unoptimized immunocomposite formation protocol; enzyme-based detection protocol; experimental proof of AgNP oxidation by hypochlorite; results and experimental details for the optimization of the immunocomposite; results demonstrating the stability of hypochlorite in water; electrochemical results for the effect of hypochlorite on the electrode surface; and a study of the stability and optimization of re-solvation time of bleach dried on paper. See DOI: 10.1039/c5lc00731c

Three previous studies are most directly related to the findings we report here. First, Limoges and coworkers have demonstrated an immunoassay wherein gold nanoparticles (AuNPs) are oxidized by Br_2 in an acidic bromine–bromide solution.[39] The resulting gold ions were electrodeposited onto a screen-printed electrode and subsequently oxidized using anodic stripping voltammetry (ASV). The charge under the ASV peak was correlated to the concentration of analyte originally present. Second, Szymanski and coworkers reported a sandwich immunoassay similar to that of Limoges, but using AgNP, rather than AuNP, labels.[40,41] After formation of the sandwich, they added the aggregating agent ammonium thiocyanate. This was thought to lead to negatively charged AgNP aggregates that could be electrostatically attracted to the electrode by applying a positive potential. The AgNPs were then directly oxidized electrochemically, the resulting Ag^+ reduced onto the electrode surface, and then, as in the Limoges experiment, oxidized by ASV. Third, our group previously demonstrated electrochemical detection of AgNP labels in a paper fluidic device using a chemical oxidant ($KMnO_4$) to spontaneously oxidize the AgNPs to Ag^+.[42] The liberated Ag^+ ions were then detected by coupling electrodeposition with subsequent ASV.

In the present article, we build upon our previous findings by carrying out a quantitative metalloimmunoassay of ricin using a 3D electrochemical PAD. The paper device itself is fabricated by paper folding and is operated by paper slipping, so we call it an origami slip PAD or *o*Slip. The detection method includes two simple but effective amplification steps that enable picomolar detection limits of the ricin *a* chain within 4.5 min. The first amplification stage involves magnetic preconcentration of AgNP labels directly at the working electrode surface. The second results from a 250 000-fold electrochemical amplification of the target concentration by combining 20 nm AgNP labels with ASV. The result is a simple-to-use and easily reconfigurable device that costs under US$0.30 (not including reagents) to produce at the lab scale and that can be remediated after use by incineration.

Experimental section

Chemicals and materials

All solutions were prepared with deionized (DI) water (>18.0 MΩ cm, Milli-Q Gradient System, Millipore, Bedford, MA). NaCl, NaOH, Whatman grade 1 chromatography paper (180 μm thick, 20 cm × 20 cm, linear flow rate (water) of 13 cm/30 min), and siliconized low retention microcentrifuge tubes, were all purchased from Fisher Scientific (Pittsburg, PA). All borate solutions were prepared by dissolving the appropriate amount of boric acid (EM Science, Darmstadt, Germany) in DI water, and then adjusting the pH with NaOH. Phosphate buffer saline (PBS, containing 10.0 mM phosphate, 138.0 mM NaCl, and 2.7 mM KCl adjusted to pH 7.5) was prepared by dissolving a package of dry PBS powder (in foil pouches from Sigma-Aldrich, St. Louis, MO) in 1.0 L of DI water. A 1.0 M phosphate buffer (PB) solution (no Cl^-) was prepared by dissolving the appropriate amount of NaH_2PO_4 and Na_2HPO_4 (Sigma-Aldrich, St. Louis, MO) in 0.50 L of DI water and then adjusting the pH with NaOH. Instant non-fat dry milk was obtained from Saco Mix'n Drink (Middleton, WI).

Ammonium sulfate, $(NH_4)_2SO_4$, and 3,3′,5,5′-tetramethylbenzidine (TMB) were purchased from Thermo Fisher Scientific (Waltham, MA). Microcut disks (1200 grit, 7.3 cm diameter) were purchased from Buehler (Lake Bluff, IL). Anti-mouse horseradish peroxidase (HRP) conjugated to antibodies were obtained from Jackson ImmunoResearch Laboratories, Inc. (West Grove, PA). Some experiments were carried out in a traditional electrochemical cell (*i.e.*, not paper) made of polytetrafluoroethylene (PTFE) (Fig. S1†). Citrate-capped AgNPs (measured diameter: 19 ± 4 nm, Fig. S2a†) and conductive Cu tape (6.3 mm wide) were purchased from Ted Pella (Redding, CA). Transmission electron microscopy (TEM) grids consisted of lacey carbon over 400 mesh Ni grids (Electron Microscopy Sciences, Hatfield, PA). Epoxy-functionalized magnetic microbeads (MμBs, Dynabeads M-270) were obtained from Invitrogen (Grand Island, NY). Erioglaucine disodium salt (blue dye) and 1,1′-ferrocene dimethanol (FcDM) were obtained from Acros Organics (Pittsburgh, PA). Sodium hypochlorite (NaClO, 13%, 1.75 M) was obtained from Fisher Science Education (Hanover Park, IL). Conductive carbon paste (Cl-2042) was purchased from Engineered Conductive Materials (Delaware, OH). Acrylic plates (0.6 cm-thick) were obtained from Evonik Industries (AcryliteFF). Microtiter plates (Costar 3590) were purchased from Sigma-Aldrich.

Ricin *a* chain was obtained from Vector Laboratories. Monoclonal *E. coli* single-chain variable fragment anti-ricin *a* chain antibody (43RCA, K_d = 0.046 nM) was synthesized using a literature protocol.[43] Monoclonal mouse anti-ricin *a* chain (AB-RIC-mAb2, K_d = 0.420 nM) was obtained from the Critical Reagent Program.[44] Anti-mouse HRP antibodies were purchased from Jackson ImmunoResearch Laboratories, Inc. Cylindrical neodymium magnets (1/16″ × 1/2″, N48) were acquired from Apex Magnets (Petersburg, WV). The following powders were used as hoax substances: Community Coffee powdered creamer, Safeway Select confectionary powdered sugar, Morton ionized salt, Fleischmann's RapidRise highly active yeast, Saco Mix'n Drink instant non-fat dry milk, Ajax powdered cleanser, Lotrimin antifungal foot powder, Johnson's baby powder, Now Solutions bentonite clay powder, Gold Medal unbleached flour, and Arm & Hammer pure baking soda.

Instrumentation

All electrochemical measurements were made using a model 700E bipotentiostat from CH Instruments (Austin, TX). The working electrode (WE), reference electrode (RE), and counter electrode (CE) used in the conventional electrochemical setup were glassy carbon (1.0 mm diameter), saturated Hg/Hg_2SO_4, and Pt wire, respectively (CH Instruments). All immunocomposite optimization experiments were performed using

an enzyme linked immunosorbent assay (ELISA) and low-retention microcentrifuge tubes, and the outcome analyzed using a Synergy H4 plate reader. Sizing of AgNPs and validation of their complete oxidation by ClO^- were carried out by transmission electron microscopy (TEM, JEOL 2010F).

A Xerox ColorQube 8570DN printer was used for wax printing. A BioShake iQ (Q Instruments) was used to control mixing during incubation. A Sorvall Legend Micro 21R centrifuge (Thermo Scientific) was used for washing during the synthesis of the anti-ricin *a* chain AB-RIC-mAB2 antibody/AgNP conjugate. The electrode stencil was cut using an Epilog laser engraving system (Zing 16). Adobe Illustrator CS6 (version 16.0.0) was used for the design of the *o*Slip and electrode stencil. The charge under the ASVs was determined by baseline correcting the ASVs using Origin Pro8 SR4 v8.0951 (Northampton, MA), integrating the area under the peaks, and then dividing by the scan rate.

*o*Slip fabrication

The *o*Slips were fabricated using a previously reported procedure with slight variations.[42] Details are provided in the ESI.†

Protocol for AgNP/antibody conjugation

The conjugation of AgNPs with anti-ricin *a* chain AB-RIC-mAB2 antibodies was performed following a protocol reported by Porter and coworkers,[45] with slight modifications. Briefly, 1.0 mL of 565.0 pM AgNP stock solution was centrifuged and resuspended in 1.0 mL of 10.0 μg mL^{-1} anti-ricin *a* chain AB-RIC-mAB2 antibody (diluted in 1.0 mM borate solution at pH 9.0). The ratio of anti-ricin *a* chain AB-RIC-mAB2 antibody to AgNPs during incubation was 1×10^5. The resulting solution was incubated for 2 h while mixing at 1500 rpm and 24 °C. Next, the AgNP/anti-ricin *a* chain AB-RIC-mAB2 antibody conjugate was washed twice by centrifuging and resuspending in 1.0 mL of 1.0 mM borate solution (pH 9.0) and then 1.0 mL of 5% w/v skim milk dissolved in 1.0 mM borate solution (pH 9.0). Note that all centrifugation steps performed were carried out at 16 600 g at 32 °C for 20 min and followed by careful removal of the supernatant. This conjugate was stored in 1.0 mL of the skim milk solution at 4 °C until used (within one week). Details about the optimization of the antibody concentration, borate solution concentration, and pH can all be found in the ESI.†

Protocol for MμB/antibody conjugation

The conjugation of MμBs with anti-ricin *a* chain 43RCA antibodies was carried out following a protocol provided by Life Technologies,[46] with some modifications. Note that unless otherwise indicated, all of the mixing steps were carried out at 1500 rpm and 24 °C on the BioShake iQ thermomixer, and all washing steps were carried out by magnetic separation. That is, by holding a magnet against the sidewall of the microcentrifuge tube for 30 s, followed by the removal of the supernatant and resuspension in the specified solution. The conjugation protocol involves six steps. First, 5.0 mg of MμBs were suspended in 1.0 mL of 0.10 M PB (pH 7.5), incubated for 10 min while mixing, and washed twice with 1.0 mL of 0.10 M PB (pH 7.5). Second, the supernatant was removed and the MμBs were resuspended in the following solutions (in the order listed) with 10 s vortexing between each solution addition: 100 μL of 0.10 M PB (pH 7.5), 100 μL of 3.0 M $(NH_4)_2SO_4$, and 100 μL of 0.50 mg mL^{-1} anti-ricin *a* chain 43RCA antibody (dissolved in 0.10 M PB, pH 7.5). The ratio of anti-ricin *a* chain 43RCA antibody to MμBs during incubation was 3.0×10^6. Third, the MμB/anti-ricin *a* chain 43RCA antibody mixture was incubated for 12–15 h while mixing at 37 °C. Fourth, the conjugate was washed once with 1.0 mL of 5% w/v skim milk (dissolved in 0.010 M PBS (pH 7.4)). Fifth, the conjugate was resuspended in 1.0 mL of buffered skim milk and incubated for 2 h while mixing to block any unbound sites on the MμBs. Sixth, the blocked conjugate was washed twice with 250.0 μL of 10.0 mM PBS (pH 7.4) and stored at 4 °C until used (within one week). The antibody concentration used in step 2 was optimized and the details (results and experimental parameters) can be found in the ESI.†

Optimized immunoassay formation protocol

The formation of the full ricin *a* chain immunocomposite was performed by first placing 20.0 μL of the MμB/43RCA anti-ricin *a* chain antibody conjugate in a microcentrifuge tube, removing the supernatant by magnetic separation, and simultaneously adding 49.0 μL of the AgNP/AB-RIC-mAb2 anti-ricin *a* chain antibody conjugate and 25.0 μL of various concentrations of ricin *a* chain (diluted in 0.10 M borate solution (pH 7.5)). Second, the resulting mixture was incubated for at least 5 min while mixing. Third, the full sandwich immunocomposite (MμB/anti-ricin *a* chain 43RCA antibody/ricin *a* chain/anti-ricin *a* chain AB-RIC-mAB2 antibody/AgNP, hereafter the "ricin immunocomposite") was washed twice with 50.0 μL of 0.10 M borate solution (pH 7.5) and analyzed using ASV. Note that all of the mixing steps were performed at 1500 rpm and 24 °C on the BioShake iQ thermomixer, and all washing steps were carried out by magnetic separation. The concentrations of both antibody conjugates were varied to maximize the ASV signal. Details about the optimization experiments are provided in the ESI.†

Anodic stripping voltammetry (ASV) in the conventional electrochemical cell

For detection of the ricin immunocomposite in the conventional electrochemical cell (Fig. S1†), a total solution volume of 225.0 μL was analyzed. The assay was carried out as follows. First, 125.0 μL of BCl (0.10 M boric acid and 0.10 M NaCl, pH 7.5), the ricin immunocomposite (50.0 μL), and 50.0 μL of chemical oxidant were added to the electrochemical cell and mixed thoroughly. After 30 s, the resulting Ag^+ was deposited by holding the WE potential at E_{dep} = −0.900 V for t_{dep} = 200 s to electrodeposit Ag onto the electrode surface. Finally, the potential was scanned from E_i

= −0.700 V to E_f = 0 V at υ = 10 mV s^{-1} to strip off the previously electrodeposited Ag.

Results and discussion

Sensor design and detection strategy

The unassembled *o*Slip PAD is shown in Scheme 1a. The sensor platform comprises four wax-patterned paper layers. Layer 1 has two reservoirs: the *Inlet* and the *Outlet*. The cellulose is removed from the *Inlet* to provide an open *via* to the lower levels of the device, but the cellulose is retained in the *Outlet* for reasons that will be explained shortly. The three carbon electrodes, from top to bottom: the working electrode (WE), counter electrode (CE), and carbon quasi-reference electrode (CQRE), are stencil-printed on the lower face of Layer 1 (face in contact with Layer 2). Layer 2 contains a *Hollow Channel*[9] and a paper reservoir loaded with a blue dye used to signal the cessation of flow through the *Hollow Channel*. Layer 3 (the *Slip Layer*)[47] contains both a *Hollow Channel* and a paper tab for dried oxidant storage (Scheme 1a, orange color). The Slip Layer is on a separate piece of paper so that the user can easily move the oxidant into the *Hollow Channel*. Finally, Layer 4 consists of a hydrophilic layer (*Hemichannel*,[48] yellow color) and a *Sink* pad that drives a continuous flow of fluid through the device until its capacity is filled. The *o*Slip is assembled by folding the paper, as indicated by the lower black arrows in Scheme 1a, to create the origami-based 3D paper device in Scheme 1b.

The assay begins by injecting the pre-formed ricin immunocomposite into the *o*Slip inlet (Scheme 1b). As the sample is driven down the *Hollow Channel* by capillary action (Scheme 1c), the ricin immunocomposite is concentrated under the first carbon electrode (WE, Scheme 1d) by the magnetic field. When flow stops, signaled by the appearance of the blue dye at the *Outlet*, the pre-dried chemical oxidant is slipped (by pulling Layer 3 until the green indicator line is exposed) into the direct proximity of the ricin immunocomposite. It is important that the *Sink* be fully saturated at this point so that the oxidant will diffuse across the *Hollow Channel* to the magnetically sequestered ricin immunocomposite rather than being swept down the channel by convection. We have found that it takes about 12 s for the pre-dried oxidant (ClO^-) to rehydrate, diffuse across the channel, and oxidize the AgNPs (Scheme 1e). Finally, the dissolved Ag^+ ions are electrodeposited on the electrode as metallic Ag for 200 s (Scheme 1f, E_{depo} = −0.9 V *vs.* CQRE) and then stripped off (Scheme 1g, E_i = −0.7 V and E_f = 0 V, υ = 10 mV s^{-1}). This results in a quantitative signal that is directly related to the amount of ricin initially added.

Selection of a chemical oxidant

As discussed in the previous section, the first step of electrochemical detection on the *o*Slip relies on chemical oxidation of the AgNP labels. In a previous proof-of-concept demonstration of the functionality of the *o*Slip,[42] we used permanganate (MnO_4^-) to oxidize AgNPs to Ag^+ prior to initiating the rest of the electrochemical detection sequence (electrodeposition of Ag and then ASV) on the *o*Slip. However, MnO_4^- has two key limitations that affect the electrochemical signal and, therefore, the sensitivity of the assay. First, MnO_4^- slowly oxidizes water to O_2, and the resulting reduced form, MnO_2, acts as a

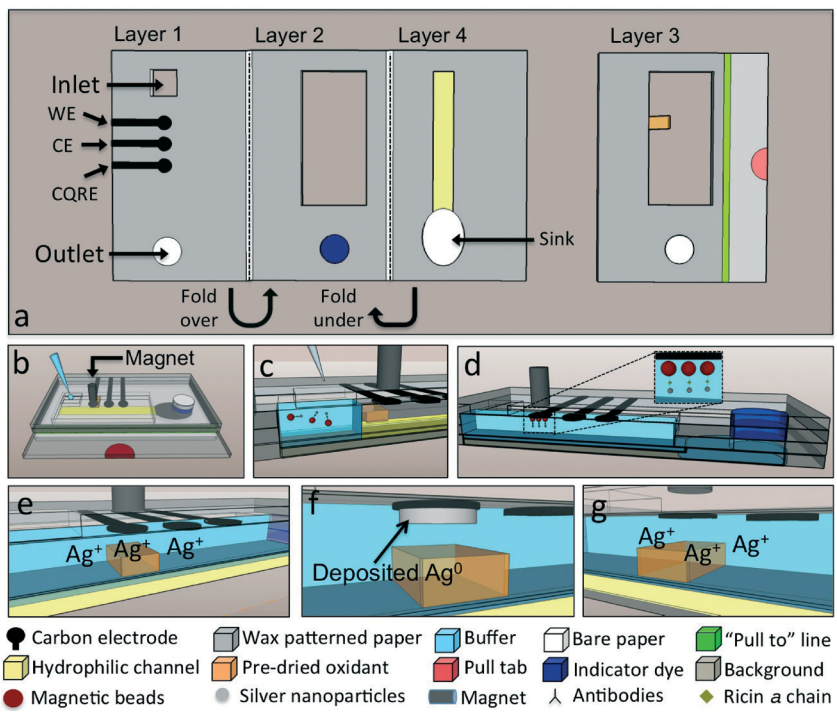

Scheme 1

catalyst for further decomposition of MnO_4^-.[49] This necessitates preparation of freshly made solutions, because the concentration of MnO_4^- is unknown following decomposition during storage. Second, MnO_4^- is known to oxidize carbon.[50,51] This results in deposition of a thin insulating layer of MnO_2 onto the working electrode, and this in turn interferes with the subsequent electrodeposition and ASV of Ag.

Because of foregoing problems, we screened a total of ten different oxidants for this study. These included the following (active oxidant in parenthesis): cerium sulfate (Ce^{4+}), potassium triiodide (I_3^-), potassium dichromate ($Cr_2O_7^{2-}$), ferric chloride (Fe^{3+}), sodium *meta*-periodate (IO_4^-), sodium perborate (BO_3^-), sodium peroxodisulfate ($S_7O_8^{2-}$), electrogenerated H_2O_2, electrogenerated Cl_2 from Cl^-, and sodium hypochlorite (ClO^-). Each of these have limitations, including: slow reaction kinetics, complexation with species in biological matrices, and instability in solution and when dried on an *o*Slip. The only chemical oxidant that proved promising, and the one used here, was ClO^-. No data are provided for the other nine oxidants tested. Hypochlorite (ClO^-) is a well-known household bleaching agent commonly used for cleaning and disinfecting. However, it has also been used in scientific research to oxidize elements and oxides such as S, Se, FeO, and SnO.[49] Additional justification for the selection of ClO^- for the present experiments is discussed in the ESI.†

Prior to carrying out experiments in the *o*Slip, we examined the effect of oxidant concentration on the Ag ASV signal in a conventional electrochemical cell. These ASV experiments were carried out as described in the Experimental section for the conventional electrochemical cell with one modification: a 50.0 μL mixture of unconjugated MμBs and citrate-capped AgNPs (2.6×10^{10} AgNPs mL^{-1} and 4.3×10^8 MμBs mL^{-1}, diluted with 0.10 M borate pH 7.5) were added to the electrochemical cell (*i.e.*, no antibodies), along with BCl and ClO^-. In this experiment the concentration of ClO^- was varied to maximize the collected charge.

Representative ASVs for this experiment are shown in Fig. 1a for three different concentrations of ClO^-. Fig. 1b is a plot of Ag ASV charge, obtained by integrating the area under ASVs like those shown in Fig. 1a, *vs.* the concentration of ClO^- used to oxidize the AgNPs. The maximum charge, located at 0.34 mM ClO^-, is a consequence of the following two factors. If the oxidant concentration is too low, then not all of the AgNPs are oxidized and the collected charge is suppressed. The effect of too much oxidant is more subtle: excess oxidant will be reduced at the working electrode during ASV, thereby leading to a high background current against which the stripping peak must be discerned. This effect is present in Fig. 1a: higher concentrations of ClO^- lead to higher background currents, which are particularly apparent between −0.4 and −0.6 V.

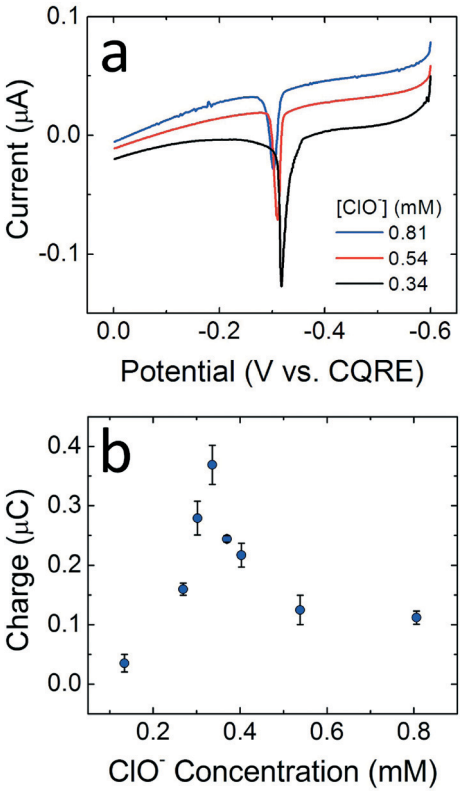

Fig. 1 (a) Three representative ASVs obtained in the conventional electrochemical cell as a function of the oxidant concentration. AgNPs (43.2 pM) were introduced into the cell and oxidized with the indicated concentrations of hypochlorite (ClO^-). The resulting Ag^+ was then electroplated onto an electrode and subsequently oxidized by ASV (scan rate: 10 mV s^{-1}). (b) Plot of the resulting charge, obtained by integration of the current under the ASV peaks, *vs.* the concentration of ClO^-. The optimal concentration of oxidant was found to be 0.34 mM. The error bars represent the standard deviation of results from three independent experiments.

Ricin detection using a conventional electrochemical cell

To benchmark the figures of merit for detection of ricin in the *o*Slip PAD, we first carried out experiments in a conventional electrochemical cell. Details regarding formation of the ricin immunocomposite, which were used for both the conventional electrochemical cell and the *o*Slip, are provided in the Experimental section, but a brief outline of the procedure is provided here (Scheme 2). First, ricin *a* chain is added to a mixture of antibody-functionalized 2.7 μm MμBs and 20 nm AgNPs to form the ricin immunocomposite in a single step (Scheme 2a), and then the mixture is allowed to incubate for 5 min. The MμBs act as a solid support that can be directed to a specified location by a magnetic field, and the AgNPs are labels that provide a 250 000-fold (the number of Ag atoms in each AgNP) amplification of the target. Eventually, we plan to incorporate these two reagents into the *o*Slip so that formation of the ricin immunocomposite can be carried out *in situ*. Therefore, the finding that the sandwich forms in a single step is important. Second, the ricin immunocomposite is washed by magnetic separation to remove unbound antibody conjugates and ricin (Scheme 2b–d). Third, the immunocomposite is resuspended in the detection buffer (Scheme 2e and f).

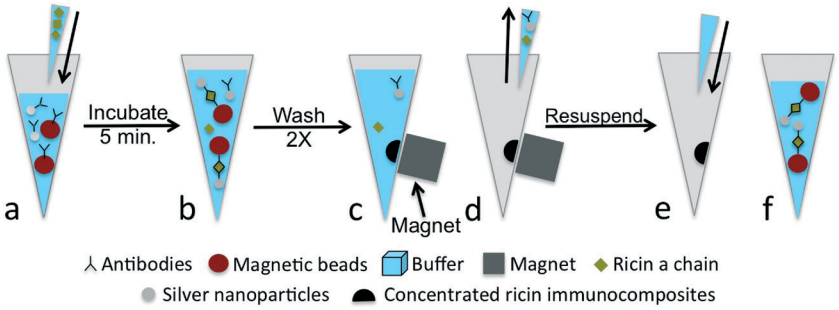

Scheme 2

Using the optimal bleach concentration (0.34 mM ClO^-) and the protocol for ASV described in the Experimental section, a range of ricin concentrations were tested: 25.0 μL of 0.0033–8.0 μg mL^{-1} ricin *a* chain, which after dilution by the AgNP/antibody solution yields a final ricin concentration range of 0.0011–2.70 μg mL^{-1}. Fig. 2a shows characteristic Ag ASVs that were used to generate the dose–response curve in Fig. 2b for ricin detection. The observed dynamic range and lowest detected amount are 0.0011 to 0.69 μg mL^{-1} (34 pM to 21 nM) and 0.0011 μg mL^{-1} (34 pM), respectively.

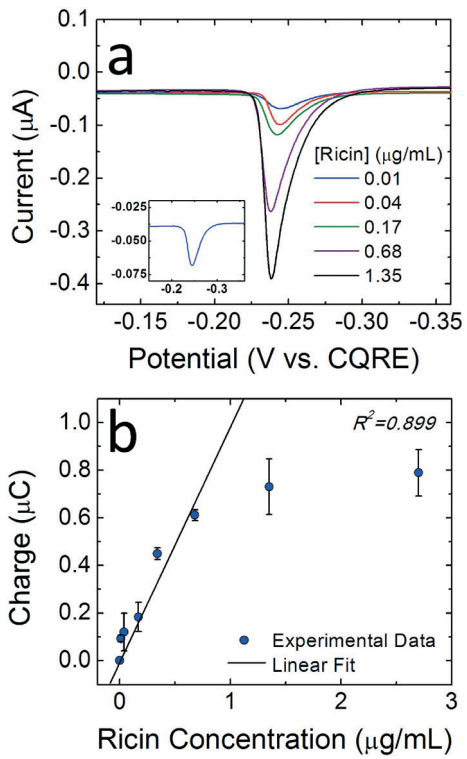

Fig. 2 Electrochemical results for detection of ricin *a* chain using the conventional electrochemical cell. (a) ASVs corresponding to immunocomposites formed using the indicated ricin concentrations (scan rate: 10 mV s^{-1}). The inset shows the ASV obtained for 0.01 μg mL^{-1} of ricin. (b) Dose–response curve, derived from data like that shown in (a), illustrating the relationship between the measured charge under the ASV peaks and the ricin concentration present during immunocomposite formation. The error bars for each data point represent the standard deviation for three independent measurements. The black line is the best linear fit to the experimental data.

Ricin detection using the *o*Slip

In preliminary *o*Slip experiments we found that the optimal concentration of oxidant determined using the conventional electrochemical cell was not sufficient for the *o*Slip. We attribute this important observation to loss of bleach activity during the drying and rehydrating processes on the paper-based reagent delivery tab of the *o*Slip (Layer 3, Scheme 1a). To optimize the bleach concentration specifically for the *o*Slip, 2.0 μL of ClO^- solutions, ranging in concentration from 1.3 to 87.4 mM, was added to the paper delivery tab and dried under a stream of nitrogen for 3 min. Next, the *o*Slip was folded into its functional configuration, and then a 50.0 μL aliquot of the ricin immunocomposite (formed using 25.0 μL of 4.0 μg mL^{-1} ricin *a* chain, which yields 1.3 μg mL^{-1} of ricin *a* chain after dilution by the AgNP/antibody solution) was injected into the *Inlet* and detected using the strategy summarized in Scheme 1. Fig. 3a shows that the optimal concentration of ClO^- for use in the *o*Slip ranges from 23.5 mM to 53.8 mM. We selected the middle of this range, 33.6 mM, for the remainder of the experiments.

To obtain a dose–response curve, a series of experiments were carried out in which the ricin immunocomposite was injected into the *o*Slip at ricin concentrations ranging from 0.011 to 2.70 μg mL^{-1}. Representative ASVs corresponding to the oxidation of Ag are shown in Fig. 3b. Importantly, each ASV was obtained using an independently fabricated *o*Slip. The fact that the peaks are so sharp and so narrowly distributed on the potential scale is remarkable for such a simple and inexpensive electrochemical device. The results also demonstrate the effectiveness of the carbon quasi-reference electrode for holding a reproducible potential under the conditions used in these experiments. Finally, notice the flat (uncorrected) baseline (compare to Fig. 1a), which simplifies integration of the ASV peaks.

A dose–response curve, constructed using raw data like that shown in Fig. 3b, is provided in Fig. 3c. The linear dynamic range is 0.0011 to 0.69 μg mL^{-1} (34 pM to 21 nM), which is exactly the same as was found for the conventional electrochemical cell. The fact that the lower end of the linear

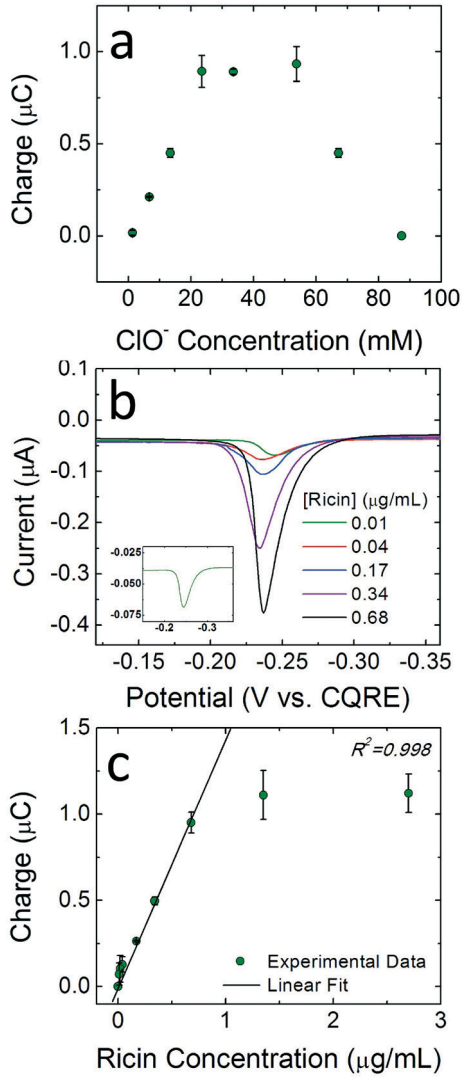

Fig. 3 Electrochemical data collected using the *o*Slip. (a) Determination of the optimal concentration of oxidant (33.6 mM ClO^-) for oxidation of the AgNP labels in the immunocomposite. The measured charge was determined from ASVs using the indicated concentrations of ClO^-. (b) ASV peaks as a function of the ricin concentration present during formation of the immunocomposite (scan rate: 10 mV s^{-1}). (c) A dose–response curve for ricin detection determined by integrating the current under ASVs, like those shown in (b), and plotting those values against the ricin concentration. The ClO^- concentration was 33.6 mM, and the lowest detectable amount of ricin *a* chain is 34.0 pM. Each data point represents an average of at least three independent measurements and the errors bars are the corresponding standard deviations. The black line is the best linear fit to the experimental data.

range is the same in both the *o*Slip and the conventional electrochemical cell is a consequence of the limiting antibody affinity. Better antibodies should lead to an even broader dynamic range in the *o*Slip due to its ability to magnetically concentrate the AgNP labels at the electrode surface. The average coefficient of variation of the data in Fig. 3c is 12.7% (average of the standard deviation divided by the mean for all concentrations of ricin), which considering that the data were obtained using 27 independently prepared *o*Slip devices is quite reasonable. At higher concentrations of ricin the dose–response curve levels off at a constant value of ~1.1 μC. This is a consequence of insufficient MμB and AgNP conjugates to bind these relatively high concentrations of ricin. Accordingly, by increasing the concentrations of the conjugates, the linear range could be extended.

Potential interferents

Powders commonly found in households are often used as hoax materials (false biothreats), and therefore it is important that a useful ricin assay not lead to a false positive result in their presence. To determine if the *o*Slip ricin assay would be adversely affected by such substances, we tested eleven common household powders, including: bentonite, powdered sugar, dry creamer, flour, dry skim milk, foot powder, table salt, yeast, baking soda, Ajax cleanser, and baby powder. Each powder was independently added (25.0 μL, 400.0 μg mL^{-1}) in the first step of the immunocomposite formation protocol (Scheme 2a) in place of ricin *a* chain. This screen was carried out using an ELISA assay, rather than using the *o*Slip, to improve throughput (details regarding the ELISA protocol are provided in the ESI†), but all other materials, including the reagents and conditions were the same.

The results of this experiment are compared to that of a ricin *a* chain (25.0 μL, 4.0 μg mL^{-1}) ELISA assay and a blank (no powder added) in Fig. 4a. Within experimental error, all of the hoax materials gave signals at the level of the blank. In contrast, the ricin *a* chain assay led to a much larger absorbance (0.26). Another interesting aspect of Fig. 4a is that the blank and hoax materials exhibited substantial backgrounds, which is typical of ELISA assays. In contrast, the electrochemical method used for the pre-formed immunocomposite in the *o*Slip is a zero-background technique (Fig. 3c). This is because AgNP/antibody conjugates (that is, AgNPs not bound to MμBs *via* ricin-induced sandwich formation) are present at such a dilute concentration that they are not detectable at the working electrode.

In addition to pure hoax materials, it is also common for biothreats involving ricin to be masked by common household powders to cloak the presence of the ricin but retain its toxicity. Accordingly, we prepared a mixture of ricin *a* chain (4.0 μg mL^{-1}) and baking soda (400.0 μg mL^{-1}, as an example), and then carried out the ASV-based electrochemical assay using the conventional electrochemical cell discussed earlier. As shown in Fig. 4b, there is no statistical difference in the Ag ASV charge collected in the presence and absence of baking soda. Therefore, the ricin *a* chain immunoassay is uncompromised, even with a common hoax material, baking soda, present in 100-fold excess.

Summary and conclusion

To summarize, we have reported a paper-based assay platform, based on the *o*Slip design shown in Scheme 1, for detection of ricin *a* chain. The approach is based on

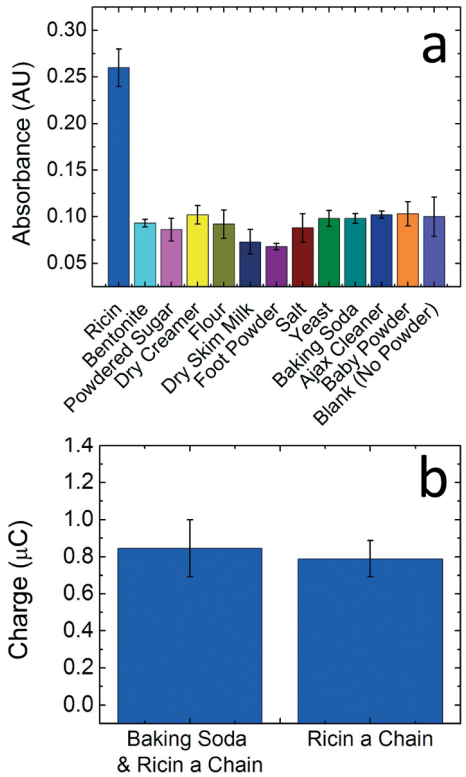

Fig. 4 Screening of potential interferents in the ricin assay. (a) Data obtained using an ELISA assay. The absorbance readings were obtained for possible interferents (no ricin present) compared to ricin-only (42.0 nM, no interferent present). A secondary antibody labeled with HRP was bound to the AgNP conjugated antibody for rapid screening (see ESI† for details). (b) A comparison of the charge collected during ASV for detection of ricin *a* chain (1.4 μg mL^{-1}, after dilution with the AgNP/antibody solution) in the presence and absence of baking soda (135.0 μg mL^{-1}, after dilution with the AgNP/antibody solution) using the conventional electrochemical cell.

quantitative, electrochemical detection of AgNP labels linked to a MμB support *via* a ricin immunosandwich. Importantly, ricin was detected at concentrations as low as 34.0 pM. Additionally, the assay is robust, even in the presence of 100-fold excess hoax materials. Finally, the device can be easily remediated after use by incineration. In the field of chemical sensing it is not common for all of these positive characteristics to manifest themselves in a device that costs just $0.30 (not including reagents) and a time-to-answer of just 9.5 min: 5 min to form the ricin immunocomposite (Scheme 2) and an additional 4.5 min for analysis on the *o*Slip (Scheme 1).

The chemical oxidant used in this assay, ClO^-, provides significantly better results than MnO_4^-, which we used in earlier proof-of-concept experiments.[42] Nevertheless, the *o*Slip still suffers from limitations. For example, the peak-shaped plot of charge *vs.* ClO^- (Fig. 3a) is not ideal, because targets that reside in matrices with easily oxidizable components, like urine or blood (which are not relevant to ricin detection), will require independent optimization. Additionally, long-term storage of the oxidant will require air-free packaging of the device. Finally, the need to manually pull the slip layer into place is not ideal. Looking to the future, we plan to focus our efforts on addressing these points.

Another virtue of the *o*Slip is that it is easily reconfigurable. Indeed, as long as appropriate antibodies are available and functional when immobilized on MμBs and AgNPs, then virtually any protein target should be quantifiable. Note, however, that we have experienced difficulty in attaching active antibodies to AgNPs, and work is ongoing in our labs to address this problem with a universal immobilization strategy. Another challenge is to eliminate the need for forming the immunocomposite *ex situ* (Scheme 2) by predispensing the MμB and AgNP immunoconjugates onto the *o*Slip at the time of device fabrication, and then resolvating them at the time of use. Finally, we will soon report that the *o*Slip can also be configured for nucleic acid detection.

Acknowledgements

This project is sponsored by the Department of the Defense, Defense Threat Reduction Agency (contract number HDTRA-1-13-1-0031). RMC thanks the Robert A. Welch Foundation (Grant F-0032) for sustained research support. JCC thanks the NASA Harriett G. Jenkins Graduate Fellowship Program, a NASA Office of Education Minority University Research and Education Program (MUREP). We gratefully acknowledge helpful discussions with Dr. Ian Richards. We also thank the Critical Reagent Program for supplying the AB-RIC-mAb2 antibody.

References

1 J. P. Fitch, E. Raber and D. R. Imbro, *Science*, 2003, **302**, 1350–1354.
2 L. Chen, D. W. McBranch, H.-L. Wang, R. Helgeson, F. Wudl and D. G. Whitten, *Proc. Natl. Acad. Sci. U. S. A.*, 1999, **96**, 12287–12292.
3 *QTL Biosystems, LLC*, 2015, http://www.azosensors.com/equipment-details.aspx?EquipID=784.
4 *ADVNT Biotechnologies*, 2015, http://www.advnt.org/products/biowarfare/baddbox.
5 J. A. Higgins, M. S. Ibrahim, F. K. Knauert, G. V. Ludwig, T. M. Kijek, J. W. Ezzell, B. C. Courtney and E. A. Henchal, *Ann. N. Y. Acad. Sci.*, 1999, **894**, 130–148.
6 *Bioveris Diagnostics*, 2015, http://www.bioveris.com.
7 U. Narang, G. Anderson, F. S. Ligler and J. Burans, *Biosens. Bioelectron.*, 1997, **12**, 937–945.
8 A. W. Martinez, S. T. Phillips and G. M. Whitesides, *Proc. Natl. Acad. Sci. U. S. A.*, 2008, **105**(50), 19606–19611.
9 C. Renault, X. Li, S. E. Fosdick and R. M. Crooks, *Anal. Chem.*, 2013, **85**, 7976–7979.
10 W. Dungchai, Y. Sameenoi, O. Chailapakul, J. Volckens and C. S. Henry, *Analyst*, 2013, **138**, 6766–6773.
11 X. Chen, J. Chen, F. Wang, X. Xiang, M. Luo, X. Ji and Z. He, *Biosens. Bioelectron.*, 2012, **35**, 363–368.
12 P. A. Larsson, S. G. Puttaswamaiah, C. Ly, A. Vanerek, J. C. Hall and F. Drolet, *Colloids Surf., B*, 2013, **101**, 205–209.

13 P. Rattanarat, W. Dungchai, D. Cate, J. Volckens, O. Chailapakul and C. S. Henry, *Anal. Chem.*, 2014, **86**, 3555–3562.
14 H. Wang, Y. Li, J. Wei, J. Xu, Y. Wang and G. Zheng, *Anal. Bioanal. Chem.*, 2014, **406**, 2799–2807.
15 S.-Q. Jin, S.-M. Guo, P. Zuo and B.-C. Ye, *Biosens. Bioelectron.*, 2015, **63**, 379–383.
16 H. Liu and R. M. Crooks, *J. Am. Chem. Soc.*, 2011, **133**, 17564–17566.
17 D. Sechi, B. Greer, J. Johnson and N. Hashemi, *Anal. Chem.*, 2013, **85**, 10733–10737.
18 G. G. Lewis, J. S. Robbins and S. T. Phillips, *Anal. Chem.*, 2013, **85**, 10432–10439.
19 H. Noh and S. T. Phillips, *Anal. Chem.*, 2010, **82**, 8071–8078.
20 E. J. Maxwell, A. D. Mazzeo and G. M. Whitesides, *MRS Bull.*, 2013, **38**, 309–314.
21 M. Novell, M. Parrilla, G. A. Crespo, F. X. Rius and F. J. Andrade, *Anal. Chem.*, 2012, **84**, 4695–4702.
22 W.-J. Lan, X. U. Zou, M. M. Hamedi, J. Hu, C. Parolo, E. J. Maxwell, P. Bühlmann and G. M. Whitesides, *Anal. Chem.*, 2014, **86**, 9548–9553.
23 L. Li, J. Xu, X. Zheng, C. Ma, X. Song, S. Ge, J. Yu and M. Yan, *Biosens. Bioelectron.*, 2014, **61**, 76–82.
24 D. Zang, L. Ge, M. Yan, X. Song and J. Yu, *Chem. Commun.*, 2012, **48**, 4683–4685.
25 Z. Nie, C. A. Nijhuis, J. Gong, X. Chen, A. Kumachev, A. W. Martinez, M. Narovlyansky and G. M. Whitesides, *Lab Chip*, 2010, **10**, 477–483.
26 H. Liu, Y. Xiang, Y. Lu and R. M. Crooks, *Angew. Chem., Int. Ed.*, 2012, **51**, 6925–6928.
27 S. Ge, W. Liu, L. Ge, M. Yan, J. Yan, J. Huang and J. Yu, *Biosens. Bioelectron.*, 2013, **49**, 111–117.
28 M. Santhiago, C. S. Henry and L. T. Kubota, *Electrochim. Acta*, 2014, **130**, 771–777.
29 P. Wang, L. Ge, M. Yan, X. Song, S. Ge and J. Yu, *Biosens. Bioelectron.*, 2012, **32**, 238–243.
30 S. Ge, L. Ge, M. Yan, X. Song, J. Yu and J. Huang, *Chem. Commun.*, 2012, **48**, 9397–9399.
31 N. Dossi, R. Toniolo, A. Pizzariello, E. Carrilho, E. Piccin, S. Battiston and G. Bontempelli, *Lab Chip*, 2012, **12**, 153–158.
32 J. C. Cunningham, N. J. Brenes and R. M. Crooks, *Anal. Chem.*, 2014, **86**, 6166–6170.
33 J. Lu, S. Ge, L. Ge, M. Yan and J. Yu, *Electrochim. Acta*, 2012, **80**, 334–341.
34 H. Zhang, D. Song, S. Gao, J. Zhang, H. Zhang and Y. Sun, *Sens. Actuators, B*, 2013, **188**, 548–554.
35 S. Zhu and W. Zhou, *J. Nanomater.*, 2010, **2010**, Article ID 562035.
36 A. Lesniewski, M. Los, M. Jonsson-Niedziółka, A. Krajewska, K. Szot, J. M. Los and J. Niedziolka-Jonsson, *Bioconjugate Chem.*, 2014, **25**, 644–648.
37 Z.-P. Chen, Z.-F. Peng, Y. Luo, B. Qu, J.-H. Jiang, X.-B. Zhang, G.-L. Shen and R.-Q. Yu, *Biosens. Bioelectron.*, 2007, **23**, 485–491.
38 Y. Luo, X. Mao, Z.-F. Peng, J.-H. Jiang, G.-L. Shen and R.-Q. Yu, *Talanta*, 2008, **74**, 1642–1648.
39 M. Dequaire, C. Degrand and B. Limoges, *Anal. Chem.*, 2000, **72**, 5521–5528.
40 M. Szymanski, A. P. F. Turner and R. Porter, *Electroanalysis*, 2010, **22**, 191–198.
41 M. Szymanski, R. Porter, G. V. Dep, Y. Wang and B. G. D. Haggett, *Phys. Chem. Chem. Phys.*, 2011, **13**, 5383–5387.
42 K. Scida, J. C. Cunningham, C. Renault, I. Richards and R. M. Crooks, *Anal. Chem.*, 2014, **86**, 6501–6507.
43 T. Pelat, M. Hust, M. Hale, M. Lefranc, S. Dübel and P. Thullier, *BMC Biotechnol.*, 2009, **9**, 60.
44 *Critical Reagent Program*, 2015, http://www.jpeocbd.osd.mil.
45 P. K. Wilson, M. Szymanski and R. Porter, *J. Immunol. Methods*, 2013, **387**, 303–307.
46 *Dynabeads® M-270 Epoxy*, 2015, https://tools.lifetechnologies.com/content/sfs/manuals/dynabeads_m270epox_man.pdf.
47 H. Liu, X. Li and R. M. Crooks, *Anal. Chem.*, 2013, **85**, 4263–4267.
48 C. Renault, J. Koehne, A. J. Ricco and R. M. Crooks, *Langmuir*, 2014, **30**, 7030–7036.
49 M. Pourbaix, *National Association of Corrosion Engineers*, 1974.
50 M. N. Patel, X. Wang, B. Wilson, D. A. Ferrer, S. Dai, K. J. Stevenson and K. P. Johnston, *J. Mater. Chem.*, 2010, **20**, 390–398.
51 D. A. Slanac, A. Lie, J. A. Paulson, K. J. Stevenson and K. P. Johnston, *J. Phys. Chem. C.*, 2012, **116**, 11032–11039.